Thermal Impact of an Active 3-D Microelectrode Array Implanted in the Brain

Sohee Kim, *Member, IEEE*, Prashant Tathireddy, Richard A. Normann, *Member, IEEE*, and Florian Solzbacher, *Member, IEEE*

***Abstract*—A chronically implantable, wireless neural interface device will require integrating electronic circuitry with the interfacing microelectrodes in order to eliminate wired connections. Since the integrated circuit (IC) dissipates a certain amount of power, it will raise the temperature in surrounding tissues where it is implanted. In this paper, the thermal influence of the integrated 3-D Utah electrode array (UEA) device implanted in the brain was investigated by numerical simulation using finite element analysis (FEA) and by experimental measurement *in vitro* as well as *in vivo*. The numerically calculated and experimentally measured temperature increases due to the UEA implantation were in good agreement. The experimentally validated numerical model predicted that the temperature increases linearly with power dissipation through the UEA, with a slope of 0.029 $^\circ$C/mW over the power dissipation levels expected to be used. The influences of blood perfusion, brain metabolism, and UEA geometry on tissue heating were also investigated using the numerical model.**

***Index Terms*—Finite element analysis (FEA), microelectrode, neural interface, neuroprosthesis, temperature increase, thermal impact, Utah electrode array (UEA).**

I. Introduction

OVER the last decades, neural prosthetic devices have been used in various applications to restore and rehabilitate disabled sensory and motor functions such as hearing, vision, limb movement, and bladder control, and to control chronic pain, spasticity, and tremor. Still, issues of safety remain about the chronic use of these active implanted devices. One safety concern of major interest is the consequence of using such implants on the heating of implanted tissues as these devices become more intelligent with the incorporation of active high-density, functional electronic components and as the number of recording and/or stimulation channels increases.

As is well known from hyperthermia therapies, temperature increases above a certain level can kill cells, change metabolism, or induce physiological abnormalities [1]–[4]. As an extreme clinical case, it is reported that a patient with an implanted deep brain stimulator (DBS) suffered significant brain damage after diathermy treatment, and subsequently died [5], [6]. In their study, postmortem examinations showed acute deterioration in the tissue near the lead electrodes of the DBS induced by excessive tissue heating. Even more moderate temperature increases in tissue can cause significant damage to various cellular functions. A temperature increase of more than 3 °C above normal body temperature has been reported to lead to physiological abnormalities such as angiogenesis or necrosis [2]. Cortical spreading depression was observed to be elicited by heating the cerebral cortex of anesthetized rats by 3.4 °C [3]. In guinea pig olfactory cortical slices, aberrant activity began at 2 °C over normal [4]. It has also been reported that temperature increases greater than 1 °C can have long-term effects on the brain tissue [7]. To prevent any of these thermal consequences, the neural interface devices must be shown not to cause significant temperature increases in the implanted tissue.

The increasing use of neuroprosthetic implants presents new potential thermal concerns. In studies on temperature elevation of the eye due to an implanted retinal stimulator [8]–[10], a 2-D model of the human eye and head was used. A finite-difference time-domain method (FDTD) was employed to predict the thermal effects of the implant. Although the authors expanded the 2-D head-eye model to a 3-D model [11], [12], their study was limited to a measurement of the *in vivo* temperature only in the center of the dog's eyeball. Their study did not show the spatial distribution of the temperature in the tissue near the implant. Also, as the position of the measurement probe was not controlled precisely, the comparison of simulated and measured temperatures might contain errors. According to their study, a 60-electrode retinal stimulator resulted in a maximum temperature rise of 0.8 °C on the surface of the chip as it dissipated a power of 12.4 mW. More recently, there has been a study reporting thermal effects of a single electrode used for deep brain stimulation (DBS) [13]. Their numerical study predicted that clinically used stimulation currents can induce temperature increases up to 1 °C near the DBS electrodes.

To the authors' knowledge, there have been no studies addressing the thermal consequences induced by the use of active 3-D microelectrode implants integrated with electronic circuitry. In this study, the thermal impact of power dissipation by implanted 3-D microelectrodes, specifically, the Utah electrode array (UEA) [14], [15] was investigated using numerical analysis as well as experimental measurement. The UEA is a 3-D silicon-based structure consisting of a 10 × 10 array of tapered

Manuscript received January 26, 2007; revised July 2, 2007; accepted August 11, 2007. This work was supported in part by NIH/NINDS Contract HHSN265200423621C and by DARPA under Contract N66001-06-C-8005.

S. Kim and P. Tathireddy are with the Department of Electrical and Computer Engineering, University of Utah, Salt Lake City, UT 84112 USA (e-mail: soheek@eng.utah.edu; p.tathireddy@utah.edu).

R. A. Normann is with the Department of Bioengineering, University of Utah, Salt Lake City, UT 84112 USA (e-mail: normann@utah.edu).

F. Solzbacher is with the Department of Electrical and Computer Engineering and the Department of Bioengineering, University of Utah, Salt Lake City, UT 84112 USA (e-mail: solzbach@ece.utah.edu).

Color versions of one or more of the figures in this paper are available online at http://ieeexplore.ieee.org.

Digital Object Identifier 10.1109/TNSRE.2007.908429

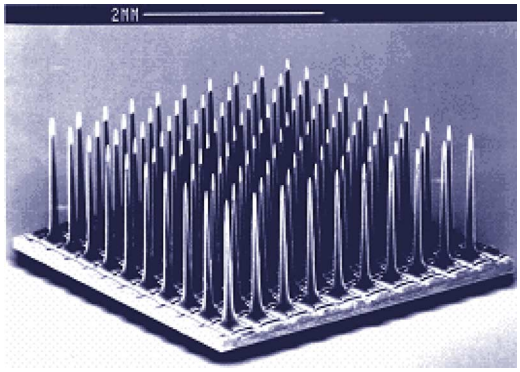

Fig. 1. Scanning electron micrograph of the UEA.

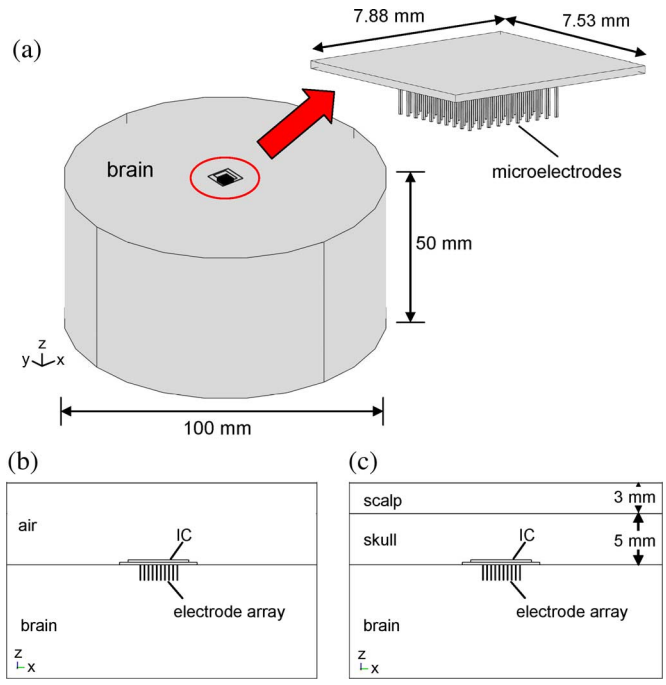

Fig. 2. (a) Modeling of the UEA and surrounding tissue for numerical simulation. Zoomed-in cross sectional view of the integrated UEA/IC system and the brain (b) not covered and (c) covered by the skull and scalp.

silicon spikes, each with a base width of 80 μm and a length of 1.5 mm, as shown in Fig. 1. Currently, progress is underway to turn the conventional wired UEA into a fully implantable wireless device [16]–[19], in which all the necessary functional components such as power source and signal processing and telemetry electronics are densely integrated with the microelectrode array. The implantable electronic circuitry is embodied in a custom designed integrated circuit (IC) [18], which amplifies and processes detected neural signals, and transmits them to an extracorporeal receiver. Since the integrated UEA/IC system dissipates a certain amount of power during operation, it will increase the temperature in surrounding tissues where it is implanted.

In Section II, the numerical and experimental methods will be described to predict the temperature increases in the brain due to power dissipation by the implanted UEA/IC integrated system. In Section III, the developed numerical model will be first validated by *in vitro* and *in vivo* measurements of temperature rises. Using the validated model, further numerical study will be performed to investigate the spatial heat distribution, the effects of blood perfusion and metabolic heat generation in the brain and UEA geometry on the temperature increases. In Section IV, conclusions will follow.

II. Methods

A. Numerical Analysis of Temperature Increases in the Brain Due to an Implanted 3-D Microelectrode Array

1) General Description of Numerical Model: Heat transfer from the implanted microelectrode array to its surrounding tissue was simulated using the finite element analysis (FEA) method. A finite element analysis software FEMLAB version 3.2b (Comsol Inc., Burlington, MA) was used. To model the thermal transport induced by a 3-D microelectrode array device, the so-called bioheat equation [20] was adapted. This model includes heat conduction, the most important mechanism of heat transfer within biomaterials [21], convection through blood flow, metabolic heat generation in the tissue, and the heat generation by the IC. In this study, only steady state heat transfer was investigated since chronic temperature rises in the tissue was of our interest. The tissues of interest were assumed to be homogeneous and isotropic. Under these assumptions, heat transfer is described based on the Pennes bioheat equation [20], by

$$\rho C\frac{\partial T}{\partial t} = k\nabla^2 T - \rho_b C_b w(T - T_b) + Q_m + Q_{\text{ext}}, \qquad (1)$$

where ρ, C, k, and T are the mass density (kg/m^3), specific heat capacity $(\text{J}/\text{kg}\cdot\text{K})$, thermal conductivity $(\text{W}/\text{m}\cdot\text{K})$, and temperature (K) of tissue, respectively. The subscript b represents values of perfusing blood. t represents time (s), w the volume flow rate of perfusing blood per unit volume ((ml/s)/ml), Q_m the metabolic heat production in the tissue (W/m^3), and Q_{ext} the external heat source (W/m^3), i.e., heat generation by the IC.

To solve the differential equation (1), the boundaries of the selected region except the surface exposed to the air was considered to be at body temperature, provided the volume to be analyzed is chosen to be sufficiently large. In this study, the volume to be analyzed was selected to be 50 mm from the array location in lateral (x-, y-) as well as vertical (z-) directions, as shown in Fig. 2(a). At the surface contacting with air, it was assumed that the heat transfer occurs in the form of free convection into air, which is described as

$$\boldsymbol{n}\cdot(k\nabla T) = h(T_{\text{ext}} - T) \qquad (2)$$

where $\boldsymbol{n}$ is the outward normal vector, h the heat transfer coefficient $(\text{W}/\text{m}^2\cdot\text{K})$, T_{ext} the external temperature (K), and k and T the thermal conductivity $(\text{W}/\text{m}\cdot\text{K})$ and temperature (K) of tissue, respectively. The temperature T_{ext} and the heat transfer coefficient h of air were assumed to be 24 °C and 5 $\text{W}/\text{m}^2\cdot\text{K}$ [22], respectively. Heat transfer by radiation at the surface into the air was neglected.

The used FEM solver was stationary linear solver using conjugate gradients method with algebraic multigrid preconditioner [22], [23]. The relative tolerance and maximum number of iteration were set to be $\varepsilon = 10^{-6}$ and 25, respectively.

2) Model Geometry: The implanted UEA/IC system was modeled in a 3-D Cartesian (x, y, z) coordinate, as shown in Fig. 2. The IC chip, as a heat source, was modeled to have a uniform heat distribution throughout the volume of $4.7 \times 5.9 \times 0.24\ \mathrm{mm}^3$. To reduce the calculation load to a level that can be coped with by the computational resource, the conical shape of electrodes was modeled as rectangular rods, each having a diameter of $80\mu\mathrm{m}$ and a length of $1500\mu\mathrm{m}$, although preliminary simulations using reduced single electrode models showed that with tapered electrode, the temperature rise was 10% greater than with rectangular electrode. Simulations using reduced single electrode models also showed that a 3-μm-thick Parylene layer that is used to insulate the electrodes of the UEA [24] increases the temperature rise by 4% compared to the model where no Parylene insulation was taken into account. Based on this result and due to the fact that it requires tremendous computational resource to calculate the thermal field of geometries with a high aspect ratio, in which the dimensions of the UEA and the insulation layer are different by 3 magnitudes of order, the effect of the electrode insulation layer was not considered in this study.

Two different models were used throughout this study: one is to validate the numerical model with experimental measurements, in which the UEA/IC system is not covered by the skull and scalp, and exposed to the air [see Fig. 2(b)]; the other is to simulate the actual implantation condition in the brain with the skull and scalp present above the implant system [see Fig. 2(c)]. The thicknesses of the scalp and skull were assumed to be 3 and 5 mm, respectively [25], as shown in Fig. 2(c). The curvature of the brain, skull, and scalp was not considered. For the brain tissue, the thickness was selected sufficiently large to be able to assume the temperature at the boundary of the selected region be equal to body temperature (37 °C). The grey matter and white matter were considered to have the same thermal and physical properties. The cerebrospinal fluid (CSF) layer between the skull and the cerebral cortex was not considered due to its relatively small thickness and the fact that the CSF likely acts as a convection mechanism. This would take heat away from heated tissue and as a consequence, the temperature rise using the model without considering CSF can be assumed to be the upper limit of maximum temperature increases.

By using mesh generation function embedded in FEMLAB version 3.2b, mesh of the models was optimized to have errors within 1% compared to the converged values using finer meshes, as shown in Fig. 3. The optimized FEA models have 78 465 tetrahedral elements and 107 256 nodes for model Fig. 2(b) and 87 299 elements and 118 325 nodes for model Fig. 2(c), resulting in a calculation time of about 60 s on a Sun X4100 server (Sun Microsystems, Santa Clara, CA).

3) Material Properties: Biomaterials such as brain, bone, or skin are usually inhomogeneous and anisotropic, and material properties such as the thermal conductivity are widely varying, depending on the measurement methods, measurement sites, and the size of samples taken for measurements [21], [26]–[31].

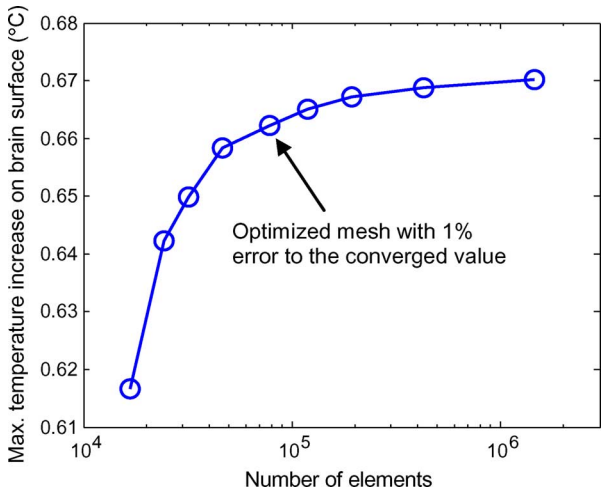

Fig. 3. Example of mesh convergence test for the thermal model in Fig. 2(b) used to predict temperature rises due to an active brain implant.

The material properties and physiological parameters of the tissues used in our study were chosen from various literature and are listed in Table I. The thermal conductivity, specific heat capacity, and mass density of tissues were mostly taken from [31], which compiles a variety of data from different primary sources [21], [26]–[30]. It is reported that the presence of blood perfusion results in a slightly higher "effective" thermal conductivity [29]. This means that the thermal conduction can occur more effectively when body fluid transports heat throughout the tissue.

The values for physiological parameters of tissues such as blood perfusion rate and metabolic heat production also vary in the literature [32]–[35]. In our study, the blood perfusion rates were taken from [33], in which the values are presented in volumetric flow rate per unit mass ((ml/min)/kg), and converted to volumetric flow rate per unit volume ((ml/s)/ml). The metabolic heat production was assumed to be 10 383, 26, and 1100 $\mathrm{W/m}^3$ for brain, skull, and scalp, respectively [35]. Besides the tissue properties, the physical and thermal properties of silicon, from which the UEA and IC are made, are also listed in Table I.

B. Experimental Measurement

Besides the numerical study described above, *in vitro* experiments were performed using a sample UEA. To mimic the heat generation by the IC, a Ti/Pt micro heating element was deposited on the backside of the UEA, as shown in Fig. 4, so that an amount of power can be supplied from an external power source and dissipated through the microelectrodes. The microheater element has a meander shape with a width/spacing of 70 $\mu\mathrm{m}$ and an effective area of $5 \times 6\ \mathrm{mm}^2$, which is equivalent to the area of the IC [18]. The thicknesses of the deposited metal films were 50 nm for Ti and 600 nm for Pt. The electrical resistance of the fabricated microheaters measured $788 \pm 3.1\ \Omega$, which was comparable to the IC's load [18]. Agarose gel (1.5%) was used to simulate the brain tissue as it has a thermal conductivity of 0.6 $\mathrm{W/(m \cdot K)}$ [31], which is similar to that of the brain. It was contained in a petri dish with 10 cm diameter and 5 mm depth. The UEA was inserted into the agarose gel so that the heat was dissipated into the volume. An amount of power

TABLE I
PHYSICAL AND PHYSIOLOGICAL PROPERTIES OF TISSUES AND ENGINEERING MATERIAL USED IN THE SIMULATIONS [31], [33], [35], [36]

	Density (kg/m^3)	Specific heat capacity (J/kg·K)	Thermal conductivity (W/m·K)	Blood perfusion rate ((ml/s)/ml)	Metabolic heat generation (W/m^3)
Brain	1041	3640	0.528	0.0097	10383
Skull	1990	1300	0.650	0.00099	26
Scalp	1100	3150	0.342	0.0022	1100
Blood	1060	3840	0.530	-	-
Silicon	2329	702	124.0	-	-

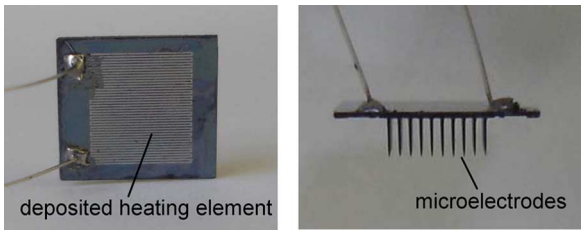

Fig. 4. Photograph of a UEA with a deposited Ti/Pt micro heating element on the backside to mimic the heat generation by the integrated IC.

TABLE II
TECHNICAL SPECIFICATIONS OF THE IR THERMAL IMAGING CAMERA USED FOR TEMPERATURE DETECTION

Measurable temperature range	-20 to 450 ºC
Wavelength	3.4 to 5 µm
Sensitivity	< 0.1º C
Spatial resolution	170 µm

from an external source (SourceMeter 2400 from Keithley Instruments, Cleveland, OH) was supplied to the micro heating element through insulated Pt wires in a diameter of 125 μm. 3 μm of Parylene was deposited on the microheater in order to protect the deposited metal trace and electrical contacts between Pt wires and the heating element.

To detect the spatial temperature distribution on the array and its surrounding medium, an infrared (IR) thermal camera (ThermaCAM PM390 from Inframetrics, currently FLIR Systems, Wilsonville, OR) was used. The technical specifications of the infrared camera are listed in Table II. The IR camera was calibrated before each set of measurements. To eliminate the distortion of thermal images due to different emission properties of Pt heating element and Si substrate [37], [38], the surface of the heating element was coated with thin black paint by spraying so that the surface emission was assumed to be close to the ideal black body. The thickness of the sprayed paint was measured to be 14.8 μm. After coating, the electrical resistance remained the same as before coating. During measurements, the temperature of the dish containing agar gel and the UEA/heater system was maintained constant in a thermally regulated water bath (Endocal RTE-8DD from Neslab, Newington, NH). The temperature of the water bath was kept at 37 °C so that the temperature at the boundary of the volume of agar gel was also kept at 37°C.

Since the *in vitro* experiment employing agar gel cannot reflect the contribution of convection through blood perfusion, which in fact plays a significant role in thermal regulation of a living body, *in vivo* experiments were also performed. The UEA/heater system was next implanted in the cerebral cortex of an anesthetized cat, as shown in Fig. 5. A small square opening (about 2×2 cm^2) was made in the skull, and the dura was removed. The cortex of the cat remained exposed during measurements. The temperature on the surface of the UEA and cortex was again measured in the steady state, using the IR thermal imaging camera.

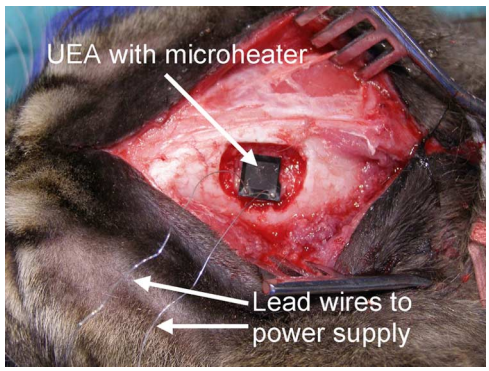

Fig. 5. *In vivo* experiment using the UEA implanted in the cerebral cortex of an anesthetized cat. Cortex of the cat remained exposed during measurements.

In both *in vitro* and *in vivo* measurements, five infrared images were taken at each level of power dissipation as the power dissipation amount ranged from 0 to 40 mW, which covers three times the range of possible power amounts dissipated though the integrated IC [18]. The representative values of the temperature distributed on the array surface were taken by spatial averaging of the detected image data in postprocessing. The five spatially averaged temperatures were again averaged at each power dissipation level. Both in *in vitro* and *in vivo* conditions, two consecutive measurements were performed and the average values of these two measurements are presented in Fig. 8.

III. RESULTS AND DISCUSSION

A. Experimental Validation of Numerical Model

An example of the calculated temperature distribution in the electrode array and its surrounding tissue is shown in Fig. 6 for a UEA/IC system that sits on the brain but not covered by the skull and scalp [see model in Fig. 2(b)]. For the simulation, the IC was modeled to dissipate a power of 13 mW, the maximum power dissipation of the IC to be expected in full operation mode [18]. Examples of the thermal images of the surface of the UEA and the surrounding medium are shown in Fig. 7 for both *in vitro* and *in vivo* conditions. In experimental measurements, the influence of the Pt lead wires on the heat transport was negligible since the resistive loss in the wires was only 0.2% of that in the heating

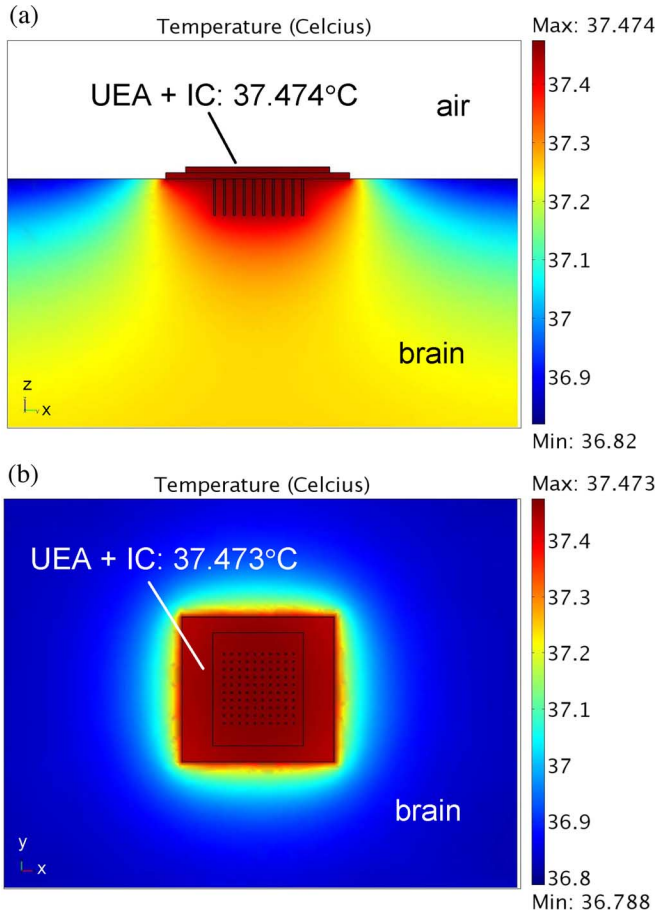

Fig. 6. Computed temperature distribution in the brain and the UEA/IC integrated system. (a) Cross-sectional view and (b) top view on the brain surface. Blood perfusion and metabolism in the brain were taken into account and the body core temperature was 37 °C. Temperature distribution was modeled for a 13 mW power dissipation, a maximum power amount expected to be dissipated by the IC.

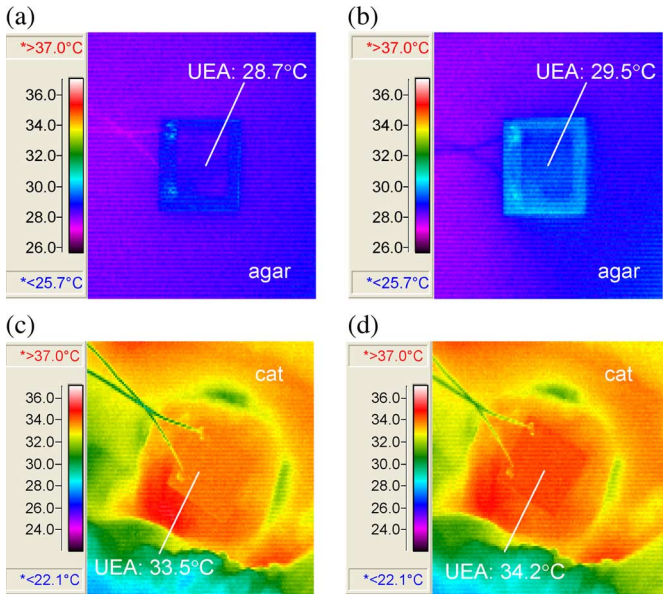

Fig. 7. Thermal images of the surface of the UEA and surrounding medium in (a) *in vitro* (agarose gel) condition with no power and (b) with 13 mW power dissipation, (c) *in vivo* (cerebral cortex of a cat) condition with no power and (d) with 13 mW power dissipation.

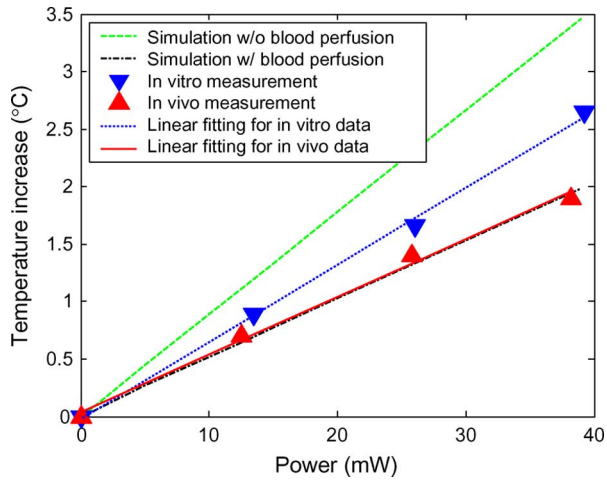

Fig. 8. Temperature increase in the UEA obtained from numerical simulations and from both *in vitro* and *in vivo* measurements as a function of power dissipation through the UEA.

element itself. Also, the conductive heat loss through the lead wires, which was observable in 2–3 mm of the soldered ends of the wires (see Fig. 7), was negligible since the volume where the heat transport occurs in the wires is much smaller than in the UEA, i.e., roughly 0.5% of the volume of the UEA.

Fig. 8 shows the maximum temperature rise as a function of the amount of power dissipation over the power dissipation range expected for an integrated UEA/IC system. The plots are from numerical simulations with and without considering perfusion, and from both *in vitro* and *in vivo* measurements. We analyzed the temperature and temperature rise on the UEA as the temperature in the surrounding medium such as tissue or agar will be no greater than the UEA temperature (see Fig. 6). It is also noteworthy that the measured temperature on the surface of tissue or agar next to the UEA, as seen in Fig. 7, is not the maximum temperature in the tissue [see Fig. 6(a)].

Numerical calculation using the model of a UEA/IC system that is not covered by the skull and scalp as shown in Fig. 6 predicted that the temperature increases linearly with power dissipation, with a slope of 0.089 °C/mW when no blood perfusion is considered and 0.051 °C/mW when blood perfusion is taken into account. The temperature increases were measured to be 0.067 °C/mW for *in vitro* and 0.050 °C/mW for *in vivo* conditions. Note that the amount of temperature rise with the increase of power dissipation was taken from the fitted lines in Fig. 8 showing the significant digits of 0.001 °C while the measured temperatures were taken with a resolution of 0.1 °C. Both *in vitro* and *in vivo* measurements were well within the computationally predicted limits; the minimum temperature increase when blood perfusion was taken into account and the maximum temperature increase when no perfusion was considered. From the numerical simulation, blood perfusion in the brain decreased the temperature rise by 42% compared to the case of no blood perfusion. The numerical simulation taking the blood perfusion into account and the measurement were in good agreement with an error of 2.5% for the *in vivo* and 29% for the *in vitro* measurements. The *in vivo* measurement showed a 22% lower temperature increase than the *in vitro* measurement, reflecting the

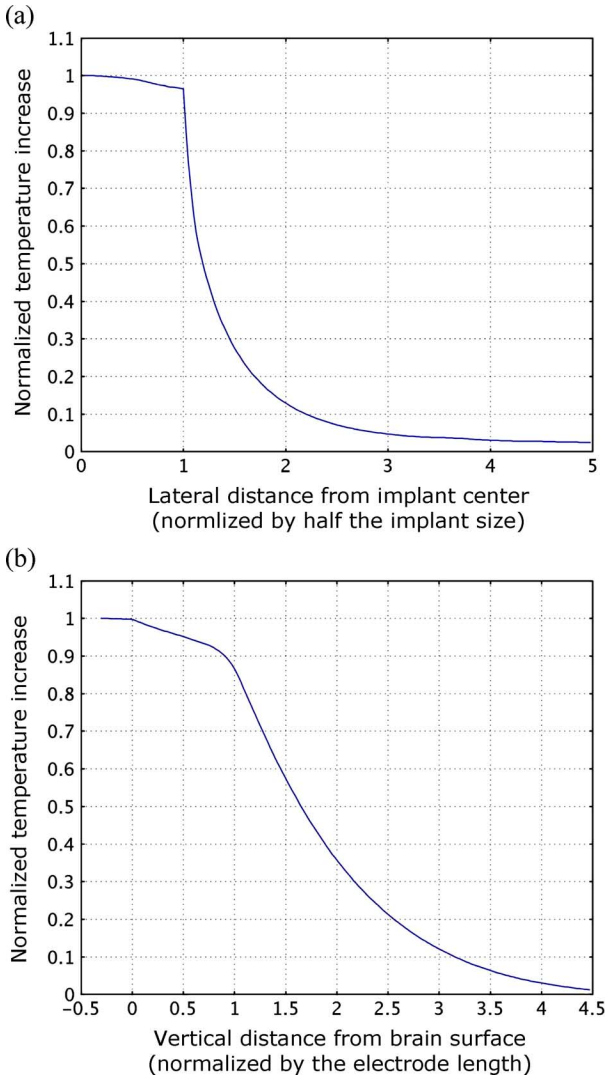

Fig. 9. (a) Temperature increase on the surface of the array and surrounding tissue due to power dissipation through the implant, normalized with maximum temperature rise that occurs at the center of the implant. Distance (along the x axis) is normalized with half the side length of the array, representing the center of the array at $x = 0$ and the edge of the array at $x = 1$. (b) Temperature increase in the tissue along with the electrode length, normalized with maximum temperature rise that occurs on top of the implant. Distance from the brain surface (along the x axis) is normalized by the electrode length, representing the electrode length from $x = 0$ to $x = 1$. Negative x axis represents the height of the UEA's base plate and the integrated IC [see Fig. 2(b) or (c)].

effect of the blood circulation in the brain removing heat away from the implanted tissue.

The good agreement of the simulated and measured results shown in Fig. 8 indicates that this numerical method can be used to further analyze the thermal impacts of the implanted microelectrode array in parametric study.

B. Numerical Results

1) Spatial Heat Distribution: Both numerical simulations and measurements employing thermal image detection on the surface of the implant system and surrounding medium suggest that only a narrow region near to the array is thermally affected by power amount dissipated through the active UEA implant (see Figs. 6 and 7). Fig. 9 shows the simulated temperature rise as a function of distance from the implant, both laterally and vertically. Fig. 9(a) shows that the temperature increase on the surface of the surrounding tissue away from the implant by half the implant size is 12% of the maximum temperature rise that occurs in the implant. In Fig. 9(b), the heating effect along with the electrode length deep in the tissue is simulated. In the tissue away from the brain surface by 2 and 3 times the electrode length, the temperature rise is 36% and 12%, respectively, of the maximum temperature increase which occurs on top of the implant system.

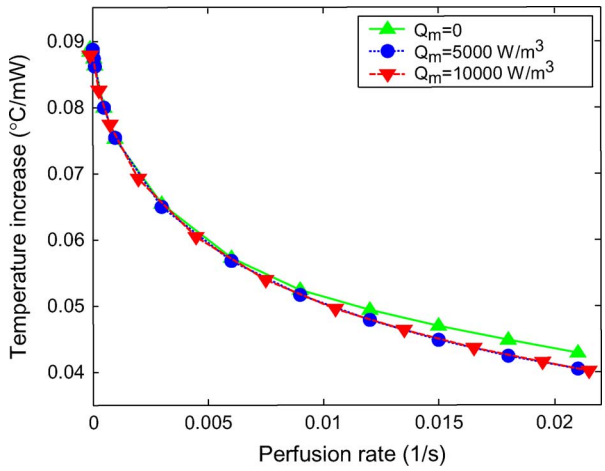

Fig. 10. Computed temperature increase in the UEA as a function of blood perfusion rate and metabolic heat generation.

2) Influence of Blood Perfusion and Metabolic Heat Generation: The results of Fig. 8 show that both numerical and experimental temperature rise observations were lower when blood perfusion was taken into account, by 42% from numerical simulation and 22% from measurement. In Fig. 10, the influence of the blood perfusion rate and metabolic heat generation on the temperature increase was simulated. Without blood perfusion, the maximum temperature increase was 0.089 $^{\circ}\mathrm{C/mW}$. When the blood perfusion of the brain was 0.009(ml/s)/ml, the temperature increase was 0.051 $^{\circ}\mathrm{C/mW}$ regardless of the metabolically generated heat amount. It is observed that the metabolic heat production in the brain does not greatly affect the temperature increase while the blood perfusion affects it significantly.

3) Influence of the Presence of Scalp and Skull Covering the Implant and the UEA Geometry: The temperature increase due to a fully implanted UEA device covered by the skull and scalp [see the model Fig. 2(c)] was simulated, as shown in Fig. 11. The maximum temperature increase using this fully implanted model resulted in 0.029 $^{\circ}\mathrm{C/mW}$, while it was 0.051 $^{\circ}\mathrm{C/mW}$ when the UEA was not covered by the skull and scalp (see Fig. 2(b) for the used model and Fig. 6 for the simulated result). When the UEA, as a heat source, is covered by thermally conductive medium such as skull and scalp, heat can be transported to the surrounding medium more efficiently. Thus, the maximum temperature on the UEA decreases.

Next, the thermal influence of the 100 electrodes of the UEA was numerically simulated, as shown in Fig. 12. The temperature increase was 0.031 $^{\circ}\mathrm{C/mW}$ when no electrodes exist (see

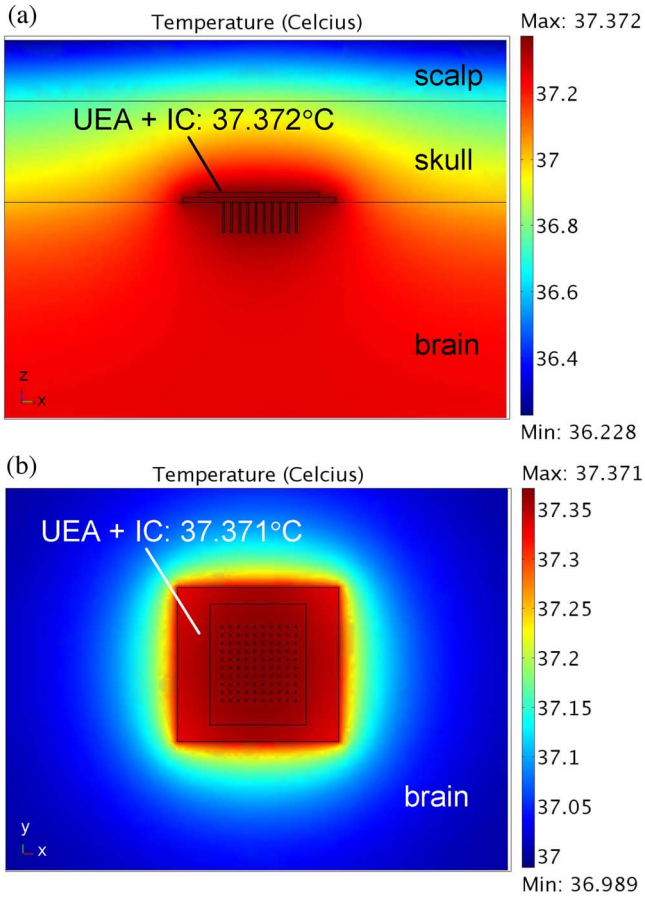

Fig. 11. Computed temperature distribution when the UEA is implanted in the cerebral cortex and covered by the skull and scalp. (a) Cross-sectional view and (b) top view on the brain surface.

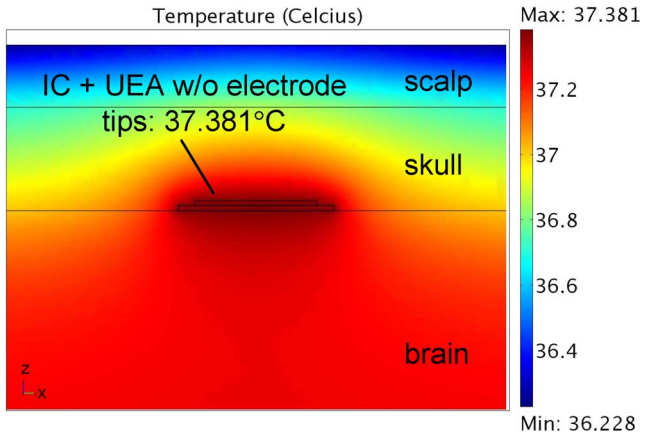

Fig. 12. Cross-sectional view of the computed temperature distribution when the UEA has no electrodes, to see the influence of the multiple electrodes of the UEA.

Fig. 12) while it was 0.029 $^{\circ}\mathrm{C}/\mathrm{mW}$ when 100 electrodes exist (see Fig. 11). The 100 microelectrodes increase the surface area of the UEA by 38%. Due to the increase in surface area contacting with the tissue through the 100 electrodes, the temperature increase was 6% less than the case where no electrodes are included. However, the increase in surface area through multiple microelectrodes does not affect the temperature rise significantly because the electrodes are populated so densely in a small volume that the thermal gradient within the volume is not that high.

IV. Conclusion

In this study, the thermal impact of a powered 3-D UEA, implanted in the brain for cortical neural signal recording, was investigated using FEA simulations and experimental *in vitro* and *in vivo* measurements. The numerical simulation using a model of the UEA that is not covered by the skull and scalp predicted that the temperature increases linearly with power dissipation through the UEA, with an amount of 0.051 $^{\circ}\mathrm{C}/\mathrm{mW}$. The numerical simulation was validated through *in vitro* and *in vivo* experiments by noninvasive temperature detection employing an IR thermal camera. The numerical calculation and experimental measurement were in good agreement. Using this experimentally validated numerical model, the temperature increase due to power dissipated by the UEA implanted in the brain and covered by the skull and scalp was predicted to be 0.029 $^{\circ}\mathrm{C}/\mathrm{mW}$. This corresponds to a temperature increase of 0.38 $^{\circ}\mathrm{C}$ for a power dissipation of 13 mW through the UEA, which is the maximum power dissipation expected by the integrated IC for our application. These results implicate that the temperature increase due to power dissipated by a 3-D UEA system implanted in the brain is in a safe range, i.e., lower than the 1 $^{\circ}\mathrm{C}$ range that is stated as the allowable temperature increase in the literature.

The spatial distribution of tissue heating, the influences of blood perfusion, metabolic heat production in the brain and UEA geometry on the temperature increase were quantitatively investigated using the developed numerical model. Although this study focuses on a specific microelectrode structure, the developed numerical model and methodology can be used to predict tissue heating due to other electrode implants of different geometries, by modifying the geometry of the numerical model.

The use of an IR camera to detect the temperature of the UEA system implanted in the tissue has the advantage that it is noninvasive, and thus allows the measurement of temperature without causing any artifacts such as bleeding that is inevitable when a temperature probe is inserted in the tissue. With this method, however, it is not possible to detect the temperature in deep tissues since it detects only surface temperatures. Also, this technique cannot be used to measure temperatures when the skull covers the implanted system. In order to gain such information, we plan to monitor the temperature of the neural interface device during operation, using an on-chip temperature sensor.

Acknowledgment

The authors would like to thank Dr. R. Harrison and Dr. L. Rieth for helpful discussions, and M. Lloyd and I. Lloyd, A. Rodriguez, and J. M. Hsu for support in array fabrication.

References

[1] W. C. Dewey, L. E. Hopwood, S. A. Sapareto, and L. E. Gerweck, "Cellular responses to combinations of hyperthermia and radiation," *Radiology*, vol. 123, pp. 463–474, 1977.

[2] T. M. Seese, H. Harasaki, G. M. Saidel, and C. R. Davies, "Characterization of tissue morphology, angiogenesis, and temperature in the adaptive response of muscle tissue in chronic heating," *Lab. Investigation*, vol. 78, pp. 1553–1562, 1998.

[3] M. Ueda, J. Bures, and J. Fischer, "Spreading depression elicited by thermal effects of ultrasonic irradiation of cerebral cortex in rats," *J. Neurobiol.*, vol. 8, pp. 381–393, 1977.
[4] T. Fujii and Y. Ibata, "Effects of heating on electrical activities of guinea pig olfactory cortical slices," *Eur. J. Physiol.*, vol. 392, pp. 257–260, 1982.
[5] P. S. Ruggera, D. M. Witters, G. von Maltzahn, and H. I. Bassen, "*In vitro* assessment of tissue heating near metallic medical implants by exposure to pulsed radio frequency diathermy," *Phys. Med. Biol.*, vol. 48, pp. 2919–2928, 2003.
[6] J. G. Nutt, V. C. Anderson, J. H. Peacock, J. P. Hammerstad, and K. J. Burchiel, "DBS and diathermy interaction induces severe CNS damage," *Neurology*, vol. 56, pp. 1384–1386, 2001.
[7] J. C. LaManna, K. A. McCracken, M. Patil, and O. J. Prohaska, "Stimulus-activated changes in brain tissue temperature in the anesthetized rat," *Metabolic Brain Disease*, vol. 4, pp. 225–237, 1989.
[8] S. C. DeMarco, G. Lazzi, W. Liu, J. D. Weiland, and M. S. Humayun, "Computed SAR and thermal elevation in a 0.25-mm 2-D model of the human eye and head in response to an implanted retinal stimulator—Part I: Models and methods," *IEEE Trans. Antennas Propag.*, vol. 51, no. 9, pp. 2274–2285, Sep. 2003.
[9] G. Lazzi, S. C. DeMarco, W. Liu, J. D. Weiland, and M. S. Humayun, "Computed SAR and thermal elevation in a 0.25-mm 2-D model of the human eye and head in response to an implanted retinal stimulator—Part II: Results," *IEEE Trans. Antennas and Propag.*, vol. 51, no. 9, pp. 2286–2295, Sep. 2003.
[10] K. Gosalia and G. Lazzi, "SAR distribution and thermal elevation in a human head model due to the operation of the data telemetry link and implanted chip in a retinal prosthesis," in *IEEE 2003 Antennas Propag. Soc. Int. Symp.*, Jun. 2003, vol. 3, pp. 1075–1078.
[11] K. Gosalia, J. Weiland, M. Humayun, and G. Lazzi, "Thermal elevation in the human eye and head due to the operation of a retinal prosthesis," *IEEE Trans. Biomed. Eng.*, vol. 51, no. 8, pp. 1469–1477, Aug. 2004.
[12] G. Lazzi, "Thermal effects of bioimplants," *IEEE Eng. Med. Biol. Mag.*, vol. 24, no. 5, pp. 75–81, Sep./Oct. 2005.
[13] M. M. Elwassif, Q. Kong, M. Vazquez, and M. Bikson, "Bio-heat transfer model of deep brain stimulation induced temperature changes," in *Proc. 28th IEEE EMBS Annu. Int. Conf.*, New York, Aug. 30–Sep. 3 2006, pp. 3580–3583.
[14] P. K. Campbell, K. E. Jones, R. J. Huber, K. W. Horch, and R. A. Normann, "A silicon-based, three-dimensional neural interface: Manufacturing processes for an intracortical electrode array," *IEEE Trans. Biomed. Eng.*, vol. 38, no. 8, pp. 758–768, Aug. 1991.
[15] K. E. Jones, P. K. Campbell, and R. A. Normann, "A glass/silicon composite intracortical electrode array," *Ann. Biomed. Eng.*, vol. 20, pp. 423–437, 1992.
[16] F. Solzbacher, R. Harrison, R. A. Normann, L. Rieth, S. Chakravarty, J.-M. Hsu, M. Klein, H. Oppermann, M. Toepper, and R. Hahn, "A next generation chronically implantable wireless neural interface," presented at the NIH/NINDS Annu. Neural Interfaces Workshop, Bethesda, MD, Sep. 7–9, 2005.
[17] M. Töpper, M. Klein, K. Buschick, V. Glaw, K. Orth, O. Ehrmann, M. Hutter, H. Oppermann, K.-F. Becker, T. Braun, F. Ebling, H. Reichl, S. Kim, P. Tathireddy, S. Chakravarty, and F. Solzbacher, "Biocompatible hybrid flip chip microsystem integration for next generation wireless neural interfaces," presented at the 56th Electronic Compon. Technol. Conf. (ECTC), San Diego, CA, May 30–June 2 2006.
[18] R. R. Harrison, P. T. Watkins, R. J. Kier, R. O. Lovejoy, D. J. Black, B. Greger, and F. Solzbacher, "A low-power integrated circuit for a wireless100-electrode neural recording system," *IEEE J. Solid-State Circuits*, vol. 42, pp. 123–133, May 2007.
[19] S. Kim, K. Zoschke, M. Klein, D. Black, K. Buschick, M. Toepper, P. Tathireddy, R. Harrison, H. Oppermann, and F. Solzbacher, "Switchable polymer based thin film coils as a power module for wireless neural interfaces," *Sensors Actuators A*, vol. 136, pp. 467–474, 2007.
[20] H. H. Pennes, "Analysis of tissue and arterial blood temperatures in the resting human forearm," *J. Appl. Physiol.*, vol. 1, pp. 93–1222, 1948.
[21] H. F. Bowman, E. G. Cravalho, and M. Woods, "Theory, measurement and application of thermal properties of biomaterials," *Ann. Rev. Biophys. Bioeng.*, vol. 4, pp. 48–80, 1975.
[22] *"COMSOL Multiphysics 3.2b User's Guide,"* FEMLAB Tutorial, 2006.
[23] K. A. Atkinson, *An Introduction to Numerical Analysis*, 2nd ed. New York: Wiley, 1988.
[24] J.-M. Hsu, S. Kammer, E. Jung, L. Rieth, R. A. Normann, and F. Solzbacher, "Characterization of Parylene-C film as an encapsulation material for neural interface devices," presented at the 3rd Annu. Conf. Multi-Material Micro Manufacture, Borovets, Bulgaria, Oct. 3–5, 2007.
[25] Y. Eshel, S. Witman, M. Rosenfeld, and S. Abboud, "Correlation between skull thickness asymmetry and scalp potential estimated by a numerical model of the head," *IEEE Trans. Biomed. Eng.*, vol. 42, pp. 242–249, 1995.
[26] H. F. Bowman, "Heat transfer and thermal dosimetery," *J. Microwave Power*, vol. 16, pp. 121–133, 1981.
[27] J. W. Valvano, J. R. Cochran, and K. R. Diller, "Thermal conductivity and diffusivity of biomaterials measured with self-heated thermistors," *Int. J. Thermophysics*, vol. 6, pp. 301–311, 1985.
[28] T. E. Cooper and G. J. Trezek, "A probe technique for determining the thermal conductivity of tissue," *ASME J. Heat Transfer*, vol. 94, pp. 133–140, 1972.
[29] J. W. Valvano, J. T. Allen, and H. F. Bowman, "The simultaneous measurement of thermal conductivity, thermal diffusivity, and perfusion in small volumes of tissue," *ASME J. Biomechan. Eng.*, vol. 106, pp. 192–197, 1984.
[30] T. A. Balasubramaniam and H. F. Bowman, "Thermal conductivity and thermal diffusivity of biomaterials: A simultaneous measurement technique," *AMSE J. Biomechan. Eng.*, vol. 99, pp. 148–154, 1977.
[31] F. A. Duck, *Physical Properties of Tissues: A Comprehensive Reference Book*. San Diego, CA: Academic, 1990.
[32] C. W. Connor and K. Hynynen, "Patterns of thermal deposition in the skull during transcranial focused ultrasound surgery," *IEEE Trans. Biomed. Eng.*, vol. 51, no. 10, pp. 1693–1706, Oct. 2004.
[33] L. R. Williams and R. W. Leggett, "Reference values for resting blood flow to organs of man," *Clin. Phys. Physiological Measurem.*, vol. 10, pp. 187–217, 1989.
[34] J. Werner and M. Buse, "Temperature profiles with respect to inhomogeneity and geometry of the human body," *J. Appl. Physiol.*, vol. 65, pp. 1110–1118, 1988.
[35] C. M. Collins, M. B. Smith, and R. Turner, "Model of local temperature changes in brain upon functional activation," *J Appl. Physiol.*, vol. 97, pp. 2051–2055, 2004.
[36] L. I. Berger, "Properties of semiconductors," in *CRC Handbook of Chemistry and Physics*, D. R. Lide, Ed., 87th ed. Boca Raton, FL: Taylor and Francis, 2006.
[37] F. P. Incropera and D. P. DeWitt, *Introduction to Heat Transfer*, 4th ed. New York: Wiley, 2002.
[38] T. J. Love, *Radiative Heat Transfer*. Columbus, OH: Merrill, 1968.

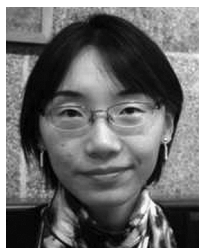

Sohee Kim (M'07) received the B.S. and M.S. degrees in mechanical engineering from the Korea Advanced Institute of Science and Technology (KAIST), Daejon, Korea, in 1998 and 2000, respectively, and the Dr.-Ing. (Ph.D.) degree in electrical engineering from the University of Saarland, Saarbruecken, Germany, in 2005.

From 2001 to 2005, she worked at the Fraunhofer Institute for Biomedical Engineering (IBMT), St. Ingbert, Germany, as a Research Engineer. She is currently a Postdoctoral Fellow in electrical and computer engineering at the University of Utah, Salt Lake City. Her research interests are wireless powering and telemetry for implantable systems such as neuroprosthetic devices, including electromagnetic and thermal aspects of such implants.

Prashant Tathireddy received the B.S. degree in chemical technology from the Osmania University, Hyderabad, India, in 1997, and the Ph.D. degree in chemical engineering from the University of Utah, Salt Lake City, in 2005.

He worked as a Project Leader in CMC, Hyderabad, India until 1999. He worked as a Postdoctoral Fellow in the Microsystems Laboratory in the Department of Electrical and Computer Engineering, University of Utah, until 2007. He is currently posted as a Guest Scientist at the Fraunhofer Institute for Biomedical Engineering (IBMT), St. Ingbert, Germany, and also holds position as a Research Assistant Professor in Electrical Engineering at the University of Utah. His research interests are development and fabrication of implantable microdevices, microfluidics, and microsensors.

Richard A. Normann (M'88) received the B.S., M.S., and Ph.D. degrees in electrical engineering from the University of California, Berkeley.

He joined the staff of the National Institutes of Health (NIH), Bethesda, MD, in 1974 and in 1979, he joined the faculty at the University of Utah, Salt Lake City. He is currently a Professor of Bioengineering and Ophthalmology. His research interests are parallel information processing in the vertebrate visual system and neuroprosthetics (the development of functional interfaces to the central and peripheral nervous system that can be used to restore lost sensory or motor function).

Florian Solzbacher (M'04) received the B.Sc. degree in electrical engineering from the University of Saarland, Germany, in 1994, the M.Sc. degree from the Technical University Berlin, in 1997, and the Ph.D. degree from the Technical University Ilmenau, in 2003.

He is co-founder of First Sensor Technology Inc., an established supplier to the automotive and process control industry in the USA, Europe, and Asia. He serves on a number of company and public private partnership advisory boards including the Center for Microsystems, ZEMI, Berlin. He is author or co-author of 70 publications and book chapters on MEMS devices, technologies, and markets and has served as (co-)organizer or Chairman of SOI and MEMS workshops and various international conferences and trade fairs, like e.g., the Sensor and Test 2005-2007 and the Advanced Microsystems for Automotive Applications International Conference AMAA in 2001, 2002, and 2003. He was a Research Associate at the Fraunhofer Institute for Biomedical Technology IBMT and the Fraunhofer Institute for Reliability and Microintegration IZM. He holds faculty positions in the Department of Electrical and Computer Engineering, Materials Science and Bioengineering at the University of Utah and is Director of the Microsystems Laboratory focusing on harsh environment microsystems and materials, including biomedical application fields. He has recently assumed responsibility for a new auxiliary branch laboratory of the Fraunhofer Institute for Reliability and Microintegration at the University of Utah.

Dr. Solzbacher is Chairman of the German Association for Sensor Technology AMA and a member of the MEMS expert advisory board to the German Ministry of Education and Research.